Fundamental Performance Limitations in Utilizing HVDC to Damp Interarea Modes

Joakim Björk, *Student Member, IEEE*, Karl Henrik Johansson, *Fellow, IEEE*, and Lennart Harnefors, *Fellow, IEEE*

***Abstract*—This paper considers power oscillation damping (POD) using active power modulation of high-voltage dc transmissions. An analytical study of how the proximity between interarea modal frequencies in two interconnected asynchronous grids puts a fundamental limit to the achievable performance is presented. It is shown that the ratio between the modal frequencies is the sole factor determining the achievable nominal performance. To illustrate the inherent limitations, simulations using a proportional controller tuned to optimize performance in terms of POD are done on a simplified two-machine model. The influence of limited system information and unmodeled dynamics is shown. The analytical result is then further validated on a realistic model with two interconnected 32-bus networks.**

***Index Terms*—Controllability, frequency control, HVDC transmission control, interarea oscillations, power oscillation damping, small-signal stability.**

I. Introduction

THE trend in today's electric power systems is increased usage of unregulated, intermittent power production from renewable sources, such as wind and solar. The ensuing reduction of inertia leads to increased concerns for the frequency stability [1]–[3]. In addition, interarea oscillations become a greater issue than in the past. High-voltage dc (HVDC) transmission is a useful technology to strengthen the grid. Its low losses makes it an attractive alternative to traditional ac transmission for longer distances. In addition, the high controllability of HVDC transmission allows the utility to actively improve power system stability by modulating active and reactive power. Since HVDC transmissions often bridge long distances, they have a strong influence on dominant power system modes. Controlling the active power, local rotor speed deviations at the HVDC terminals can be reduced, thereby improving power oscillation damping (POD) [4]–[17]. In [7] a decentralized control method was developed to improve POD through a multi-terminal high voltage dc (MTDC) system connected to an ac grid. Active power was controlled at the dc terminal with strongest controllability of the oscillatory mode. Voltage droop controllers, at the remaining dc terminals, were then tuned to maximize POD without the need of communication between the terminals. In [18], [19] the inverters of an MTDC network is controlled as virtual synchronous generators. With local ac frequency feedback the inverter can mimic the inertial response of a synchronous machine by utilizing the energy stored in the dc capacitors. The resulting dc voltage change is then compensated by redistributing power using voltage droop control, avoiding the need for communication.

Contrary to traditional ac transmission, HVDC enables the interconnection of asynchronous grids. Active-power modulation, if made fast enough, allows for the networks to share primary control reserves, reducing the maximum frequency fall (the nadir) and the steady-state frequency deviation following disturbances in load or production [5], [13], [20]. This facilitates a higher penetration of renewable power production, where inertia and primary reserves are important concerns [3].

In a case study of a future North Sea grid, Ndreko *et al*. [17] describe how HVDC active power modulation can be utilized to improve a poorly damped oscillatory mode of 0.5 Hz in the U.K. grid. This, however, results in a disturbance propagating through the North Sea HVDC network, exciting a poorly damped interarea mode of 0.5 Hz in the Nordic grid at the other end. The interaction between the interconnected ac systems can be mitigated by utilizing the wind power resources in the North Sea grid [17] or in the dc capacitors [18], [19]. The latter method may however increase the cost of the dc installation since larger capacitors may be needed. In addition such control methods require careful tuning since the introduced dc dynamics may interact with the ac system and degrade POD performance [21].

The proximity in frequency of two poorly damped oscillatory modes can be troublesome, since it greatly affects the controllability of the interarea modes and therefore impairs the achievable POD from HVDC active power modulation. This *modal interaction* is the main focus of the paper. In [5] it is shown that HVDC primary frequency control never decreases POD under some simplifying assumptions. This is proven by using a simple proportional droop controller, phase compensated for the HVDC active power actuation lag, with feedback from local frequency measurements at the two HVDC terminals. Such a

Manuscript received January 9, 2018; revised May 14, 2018 and September 6, 2018; accepted October 11, 2018. Date of publication October 17, 2018; date of current version February 18, 2019. This work was supported in part by the Knut and Alice Wallenberg Foundation, in part by the Swedish Research Council, and in part by the Swedish Foundation for Strategic Research. This work was done under the Ph.D. program in the digitalization of electric power engineering, KTH Royal Institute of Technology. Paper no. TPWRS-00044-2018. *(Corresponding author: Joakim Björk.)*

J. Björk and K. H. Johansson are with the School of Electrical Engineering and Computer Science, KTH Royal Institute of Technology, 100 44 Stockholm, Sweden (e-mail: joakbj@kth.se; kallej@kth.se).

L. Harnefors is with the School of Electrical Engineering and Computer Science, KTH Royal Institute of Technology, 100 44 Stockholm, Sweden, and also with ABB Corporate Research 721 78, Västerås, Sweden (e-mail: lennart.harnefors@se.abb.com).

Digital Object Identifier 10.1109/TPWRS.2018.2876554

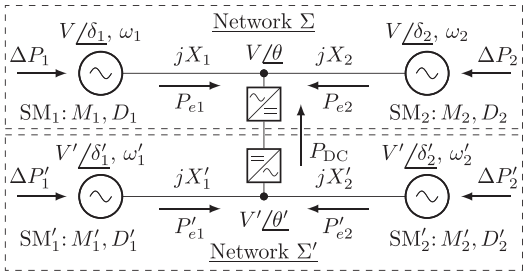

Fig. 1. The HVDC-interconnected system used to study modal interaction, between two ac networks Σ and Σ'.

control allows for efficient sharing of inertial response and primary reserves between the connected systems using only local measurements. In general, dc dynamics are orders of magnitude faster than interarea modes. For the remainder of this paper, dc dynamics will therefore be neglected. Instead, the focus will be on interactions occurring between asynchronous ac systems interconnected with HVDC.

The main contribution of this paper is to show how modal interaction limits the achievable POD from HVDC active power modulation. Due to the complexity and high order of the power systems, almost all works addressing POD rely on numerical studies. Although necessary for practical application, resorting to a numerical representation sacrifices physical intuition. In this study we build on the analytical approach of [4]–[6] with the aim of achieving more insight into the problem at hand. We let each ac network be represented by a two-machine model to characterize the dominant interarea mode in each network. The networks are connected with a single HVDC link, as shown in Fig. 1. This model, being the focus of the study, is referred to as the *HVDC-interconnected system*. A fundamental measure for how hard it is to control the interarea oscillations, independent of control structure, is obtained using the controllability Gramian [22], [23]. For the analysis, a model reduction is made to isolate the dynamics of interest. The result is a state-space model that exclusively represents the energy of the interarea oscillation in each network. It is found that the ratio between modal frequencies in each network is the only factor that determines obtainable POD benefits. The results are verified by nonlinear simulations using a droop controller tuned to optimize performance in terms of POD in both ac networks. The sensitivity to model uncertainty is also investigated. Sharing of primary reserves, e.g., to reduce the nadir, is implemented independently of the POD. In Section VI-B the analytical result is further verified by simulations using a realistic 32-bus model for each of the HVDC-interconnected networks.

The remainder of the paper is organized as follows. In Section II nonlinear and linear models of the HVDC-interconnected system are defined. In Section III, reduction of the linear model is done along with an energy interpretation. In Section IV, controllability analysis of the reduced model is made. In Sections V and VI a droop controller is synthesized and implemented in simulations to show POD performance and sensitivity. Section VII concludes the paper with some discussion of future work.

II. Model of the HVDC-Interconnected System

Consider the HVDC-interconnected system in Fig. 1. We let the dominant interarea mode in network Σ (top) and Σ' (bottom) be represented by two SMs connected by an ac transmission line. Next we derive the dynamics of Σ. Network Σ' is structurally identical to Σ but may have differing parameter values. To indicate this, parameters and variables of Σ' are referred to using prime notation.

The electromechanical dynamics for Σ are given by the swing equation

$$\begin{aligned}\dot{\delta}_i &= \omega_i \\ M_i\dot{\omega}_i &= \Delta P_i - \underbrace{\frac{V^2}{X_i}\sin\left(\delta_i-\theta\right)}_{P_{ei}} - D_i\omega_i \end{aligned} \tag{1}$$

for SM_i, $i = 1, 2$. Machines are modeled, using the classical machine model, as a stiff electromotive force behind a transient reactance [2]. Machine excitation and reactive-power at the HVDC terminal are controlled (using, e.g., a voltage-source converter HVDC terminal, a static var compensator, or a variable shunt capacitor bank) so that all buses have the voltage amplitude V for the time frame of interest. The machine busbar-voltage phase angles are given by δ_i. The variable ω_i represents machine i's deviation from the nominal frequency $\omega_s = 2\pi f_s$, where f_s is usually 50 or 60 Hz. The constant M_i represents the frequency and pole-pair scaled inertia of each machine. Higher-order dynamics such as impact from machine damper windings, voltage regulators and system loads, governors etc. are lumped into the damping constant D_i. Transmission is assumed lossless and the electrical distance between machine i and the dc bus is represented by the reactance X_i, consisting of transient machine reactance, transformers, and transmission lines, The difference between the mechanical input power from the machines and the local loads is given by ΔP_i. DC busbar-voltage phase angle θ is given by the active-power balance

$$P_{\mathrm{DC}} + \sum_{i=1}^{2}\frac{V^2}{X_i}\sin\left(\delta_i-\theta\right) = 0 \tag{2}$$

where P_{DC} is active power injected at the HVDC terminal.

Linearization and further simplifications in line with those of [5] are made next. SM_2 is set as the phase reference without loss of generality: $\delta_2 = 0$, $\delta = \delta_1 - \delta_2$, and $\dot{\delta} = \omega_1 - \omega_2$. Assuming small power flows, with $\Delta P_i \approx 0$, gives small voltage phase-angle differences between buses. For the linear study we then simplify $\sin\left(\delta_i-\theta\right) \approx \delta_i - \theta$ in (1) and, similarly, from (2) then approximately

$$\theta = \frac{X_2}{X_{12}}\delta + \frac{X_1X_2}{V^2X_{12}}P_{\mathrm{DC}} \tag{3}$$

where $X_{12} \triangleq X_1 + X_2$. These simplifications result in the linear state-space model

$$\begin{aligned}\dot{x} &= A_x x + B_x u \\ y &= C_x x \end{aligned} \tag{4}$$

with state vector $x = \left[\, \delta,\ \omega_1,\ \omega_2 \,\right]^{\mathsf{T}}$, input $u = P_{\mathrm{DC}}$, and y some output yet to be defined.

For the study of POD and modal interaction, additional simplifications are possible without loss of relevant dynamics. This will be essential in order to analytically analyze the HVDC-interconnected system. Since only the electro-mechanical oscillations between the two machines are of interest, only frequency in relation to the center of inertia (COI) frequency

$$\omega_{\mathrm{COI}} = \frac{M_1}{M_{12}}\omega_1 + \frac{M_2}{M_{12}}\omega_2 \tag{5}$$

where $M_{12} = M_1 + M_2$, needs to be considered. We therefore let the output vector be $y = \left[\, \delta,\ \omega_1 - \omega_{\mathrm{COI}},\ \omega_2 - \omega_{\mathrm{COI}} \,\right]$. Additionally, we assume that the machine damping is evenly distributed and proportional to the machine inertia

$$D_i = D\frac{M_i}{M_{12}} \tag{6}$$

such that the machines become scaled versions of each other. System matrices in (4) are then given by

$$A_x = \begin{bmatrix} 0 & 1 & -1 \\ \frac{-V^2}{M_1 X_{12}} & \frac{-D}{M_{12}} & 0 \\ \frac{V^2}{M_2 X_{12}} & 0 & \frac{-D}{M_{12}} \end{bmatrix},\ B_x = \begin{bmatrix} 0 \\ \frac{X_2}{M_1 X_{12}} \\ \frac{X_1}{M_2 X_{12}} \end{bmatrix},$$

$$C_x = \begin{bmatrix} 1 & 0 & 0 \\ 0 & \frac{M_2}{M_{12}} & \frac{-M_2}{M_{12}} \\ 0 & \frac{-M_1}{M_{12}} & \frac{M_1}{M_{12}} \end{bmatrix}. \tag{7}$$

III. Model Reduction and Energy Interpretation

In this section we discuss how to reduce the state dimension of the model introduced previously, and how to make a useful energy interpretation of the model.

Thanks to the assumption (6), the two machines are linearly scaled versions of each other. Therefore, only machine frequency deviations, scaled by M_1 resp. M_2, around ω_{COI} are observable in y. Hence, only the difference $\omega_1 - \omega_2$ (and not the absolute states) is observable. Thus the model (7) is not a minimal realization but can be reduced further without losing additional control information [22].

A. Model Reduction

Let $P^{\dagger}$ be the Moore-Penrose pseudoinverse of a time invariant 3×2 transformation matrix P, and let z be the reduced 2×1 state vector from the linear transformation $z = P^{\dagger}x$. A minimal realization of (4) is then

$$\begin{aligned} \dot{z} &= A_z z + B_z u \\ y &= C_z z \end{aligned} \tag{8}$$

where $A_z = P^{\dagger}A_x P$, $B_z = P^{\dagger}B_x$ and $C_z = C_x P$ [22]. There are infinitely many choices of P. A good choice, highlighting the dynamics of interest is to let

$$P^{\dagger} \triangleq \begin{bmatrix} 1 & 0 & 0 \\ 0 & 1 & -1 \end{bmatrix}. \tag{9}$$

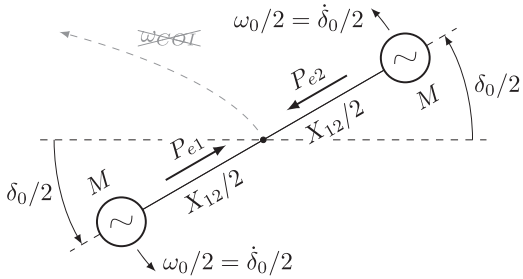

Fig. 2. Visualization of the reduced linearized symmetric ac network Σ.

With this choice, the reduced state vector becomes $z = \left[\, \delta,\ \omega \,\right]^{\mathsf{T}}$ where $\omega = \omega_1 - \omega_2$. The matrices in (8) become

$$A_z = \begin{bmatrix} 0 & 1 \\ \frac{-V^2 M_{12}}{M_1 M_2 X_{12}} & \frac{-D}{M_{12}} \end{bmatrix},\ B_z = \begin{bmatrix} 0 \\ \frac{M_2 X_2 - M_1 X_1}{M_1 M_2 X_{12}} \end{bmatrix},$$

$$C_z = \begin{bmatrix} 1 & 0 & 0 \\ 0 & \frac{M_2}{M_{12}} & \frac{-M_1}{M_{12}} \end{bmatrix}^{\mathsf{T}} \tag{10}$$

with undamped frequency

$$\omega_0 = 2\pi f_0 = \sqrt{\frac{V^2 M_{12}}{M_1 M_2 X_{12}}}. \tag{11}$$

This construction can be compared to the classical two-body problem of Newtonian mechanics [24]. From (10) it is easily seen that the interarea mode is controllable using active power injection, as long the HVDC terminal is not located at the mass-scaled electrical midpoint between the two machines, i.e., as long as $M_1 X_1 \neq M_2 X_2$. This agree with the findings of [4]–[6]. To simplify the analysis further, consider the special case $M_1 = M_2 = M$, which we refer to as a *symmetric network*. The system matrices become

$$A_z = \begin{bmatrix} 0 & 1 \\ \frac{-2V^2}{M X_{12}} & \frac{-D}{2M} \end{bmatrix},\ B_z = \begin{bmatrix} 0 \\ \frac{X_B}{M} \end{bmatrix},\ C_z = \begin{bmatrix} 1 & 0 \\ 0 & 0.5 \\ 0 & -0.5 \end{bmatrix} \tag{12}$$

where $X_B = \frac{X_2 - X_1}{X_{12}} \in [-1, 1]$ is the electric position of the dc bus w.r.t. line impedance.

B. Energy Interpretation

Interarea oscillations (or power oscillations) are electric power being transfered between machines.

Consider the unforced, undamped symmetrical ac network shown in Fig. 2, where the swing equation (1) gives

$$M\dot{\omega}_0 = -2P_{ei} = -\frac{V^2}{X_{12}/2}\delta_0,\ i = 1,\ 2. \tag{13}$$

Work is the conversion between mechanical kinetic energy and electrical potential energy. Hence, power oscillations are an electromechanical phenomenon. Multiplying both sides in (13) by $d\delta/dt = \omega$ and deriving work done to both machines as the integral of power over time, t, we get

$$2\int M\omega_0 \frac{d\omega_0}{dt}dt = -2\int \frac{V^2}{X_{12}/2}\delta_0 \frac{d\delta_0}{dt}dt \tag{14}$$

or

$$\frac{2V^2}{X_{12}}\delta_0^2 + M\omega_0^2 = E_p + E_k \triangleq E_0 \tag{15}$$

where, since we are dealing with a conservative system, the sum of kinetic $E_k = M\omega_0^2$ and potential energy $E_p = \frac{2V^2}{X_{12}}\delta_0^2$ is constant over time [24]. This sum is referred to as the *oscillatory energy* E_0, which is the quantity we are interested in controlling using active power injection at the dc terminal.

C. Modeling the HVDC-Interconnected System

Using (8) together with (10) or (12), the HVDC-interconnected system in Fig. 1 can now be described by

$$\dot{\boldsymbol{z}} \triangleq \begin{bmatrix} \dot{z} \\ \dot{z}' \end{bmatrix} = \begin{bmatrix} A_z & 0 \\ 0 & A_z' \end{bmatrix} \begin{bmatrix} z \\ z' \end{bmatrix} + \begin{bmatrix} B_z \\ B_z' \end{bmatrix} \boldsymbol{u} \triangleq \boldsymbol{A}_z \boldsymbol{z} + \boldsymbol{B}_z \boldsymbol{u} \tag{16}$$

where variables and parameters referring to the HVDC-interconnected system are with boldface letters.

IV. Controllability Analysis

As long as the controllability matrix have full rank, the system is controllable. To assess on how hard the system is to control, we will use the controllability Gramian of (16) defined by

$$\boldsymbol{W}_C = \int_0^T e^{\boldsymbol{A}_z t} \boldsymbol{B}_z \boldsymbol{B}_z^{\mathsf{T}} e^{\boldsymbol{A}_z^{\mathsf{T}} t} dt. \tag{17}$$

The system is controllable if and only if $\boldsymbol{W}_C$ is nonsingular for any $T > 0$ [23]. If $D,\ D' > 0$ then $\boldsymbol{A}_z$ is Hurwitz, i.e., its eigenvalues have strictly negative real part. The controllability Gramian $\boldsymbol{W}_C$ over infinite time, $T = \infty$, is then given by the unique solution to the Lyapunov equation

$$\boldsymbol{A}_z \boldsymbol{W}_C + \boldsymbol{W}_C \boldsymbol{A}_z^{\mathsf{T}} + \boldsymbol{B}_z \boldsymbol{B}_z^{\mathsf{T}} = 0. \tag{18}$$

The controllability Gramian gives us the minimal energy control, or *control effort*, required to transfer the system from one state to another. The control effort required to transfer an initially disturbed system state, $\boldsymbol{z}(t=0) = \boldsymbol{z}_0$, to the origin, $\boldsymbol{z}(t \to \infty) = 0$, is given by

$$\|\boldsymbol{u}\|_2^2 = \boldsymbol{z}_0^{\mathsf{T}} \boldsymbol{W}_C^{-1} \boldsymbol{z}_0 \tag{19}$$

where $\boldsymbol{u} \in L_2[0,\ \infty)$ [23]. The singular value decomposition [22] of $\boldsymbol{W}_C$ is

$$\boldsymbol{W}_C = \boldsymbol{V} \boldsymbol{\Sigma} \boldsymbol{V}^{\mathsf{T}} \tag{20}$$

where $\boldsymbol{\Sigma}$ is a diagonal matrix with singular values $\boldsymbol{\sigma}_1 \leq \ldots \leq \boldsymbol{\sigma}_4$ on its diagonal, and $\boldsymbol{V}$ is an orthogonal unitary matrix ($\boldsymbol{V}^{-1} = \boldsymbol{V}^{\mathsf{T}}$) with column vectors $\boldsymbol{v}_i$, $i = 1, 2, 3, 4$ being the singular vectors. With $\boldsymbol{z}_i \triangleq \boldsymbol{v}_i^{\mathsf{T}} \boldsymbol{z}_0$ it follows that the control effort can be computed as

$$\|\boldsymbol{u}\|_2^2 = \boldsymbol{z}_0^{\mathsf{T}} \boldsymbol{V} \boldsymbol{\Sigma}^{-1} \boldsymbol{V}^{\mathsf{T}} \boldsymbol{z}_0 = \sum_{i=1}^{4} \frac{\boldsymbol{z}_i^2}{\boldsymbol{\sigma}_i}. \tag{21}$$

A. Assessing Controllability of an Isolated AC Network

Consider the single ac network Σ in (12) with $D > 0$, controlled with an arbitrary active power injection at the dc bus from a source with negligible dynamics, e.g., a large battery storage. The controllability Gramian for Σ is

$$W_C^{\Sigma} = \begin{bmatrix} \frac{X_B^2}{D}\frac{X_{12}}{2V^2} & 0 \\ 0 & \frac{X_B^2}{D}\frac{1}{M} \end{bmatrix} \begin{matrix} \delta \\ \omega \end{matrix}. \tag{22}$$

According to (21), the control effort required to transfer the system from an initially disturbed state to zero is given by

$$\|u\|_2^2 = z_0^{\mathsf{T}} \left(W_C^{\Sigma}\right)^{-1} z_0 = \frac{D}{X_B^2}\frac{2V^2}{X_{12}}\delta_0^2 + \frac{D}{X_B^2} M\omega_0^2 \tag{23}$$

where δ_0 and ω_0 are the system state variables corresponding to the energy of the disturbance (15). Expressing (23) in the terms of oscillatory energy (15), we get

$$\|u\|_2^2 = \frac{D}{X_B^2}(E_p + E_k) = \frac{D}{X_B^2} E_0. \tag{24}$$

Here it is seen that control effort is inversely proportional to the squared (mass-weighted) electric position, X_B^2, of the dc terminal. This agrees with the findings of [4]–[6].

Remark 1: If we let $D = 0$, then the finite-time Gramian (17) gives us an intuitive interpretation of the required control effort (19). The time, T, is a measure of the control aggressiveness.

B. Computing the Gramian $\boldsymbol{W}_C$

The controllability Gramian (18) for the HVDC-interconnected system, computed using Kronecker products [25] in MATLAB's Symbolic Math Toolbox yields

$$\boldsymbol{W}_C \equiv \begin{bmatrix} a & -\boldsymbol{\alpha} & 0 & -\boldsymbol{\gamma} \\ -\boldsymbol{\alpha} & a' & \boldsymbol{\gamma} & 0 \\ 0 & \boldsymbol{\gamma} & b & -\boldsymbol{\beta} \\ -\boldsymbol{\gamma} & 0 & -\boldsymbol{\beta} & b' \end{bmatrix} \begin{matrix} \delta \\ \delta' \\ \omega \\ \omega' \end{matrix}. \tag{25}$$

Note that the rows and columns have been rearranged according to the column of state variables on the right in order to clarify the result. The elements of (25) depend on the parameters of Σ and Σ'. The main factor determining controllability is the undamped modal frequencies ω_0 and ω_0' in (11).

For the following analysis we choose

$$M' \triangleq M + \epsilon \tag{26}$$

and let Σ and Σ' be identical in all other aspects. Note that $\omega_0 \neq \omega_0'$ if $\epsilon \neq 0$. The elements of (25) are then given by

$$\begin{aligned} a = a' &= \frac{X_B^2}{D}\frac{X_{12}}{2V^2},\ b = \frac{X_B^2}{D}\frac{1}{M},\ b' = b\frac{M}{M+\epsilon}, \\ \boldsymbol{\alpha} &= a\frac{2M+\epsilon}{2M+\epsilon+2c\epsilon^2},\ \boldsymbol{\beta} = b\frac{2M}{2M+\epsilon+2c\epsilon^2}, \\ \boldsymbol{\gamma} &= \frac{X_B^2}{D^2}\frac{2\epsilon}{2M+\epsilon+2c\epsilon^2},\ c = \frac{2V^2}{D^2 X_{12}}. \end{aligned} \tag{27}$$

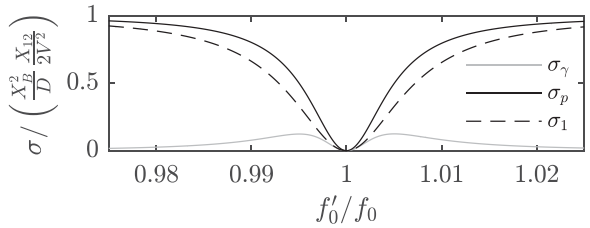

Fig. 3. Estimated singular values $\boldsymbol{\sigma}_\gamma$ and $\boldsymbol{\sigma}_p$ together with numerically calculated $\boldsymbol{\sigma}_1$. Modal frequencies f_0' and f_0 according to (11) and (26).

Here we note that $\boldsymbol{\alpha} \to a = a'$, $\boldsymbol{\beta} \to b$, $b' \to b$, and $\gamma \to 0$, as $\epsilon \to 0$, which make $\boldsymbol{W}_C$ rank deficient. Moreover,

$$\begin{matrix} \boldsymbol{v}_1 & \boldsymbol{v}_2 & \boldsymbol{v}_3 & \boldsymbol{v}_4 \end{matrix}$$

$$\lim_{\epsilon \to 0} \boldsymbol{V} = \frac{1}{\sqrt{2}} \begin{bmatrix} 1 & 0 & 1 & 0 \\ 1 & 0 & -1 & 0 \\ 0 & 1 & 0 & 1 \\ 0 & 1 & 0 & -1 \end{bmatrix} \begin{matrix} \delta \\ \delta' \\ \omega \\ \omega' \end{matrix}. \tag{28}$$

As can be expected for the control of a multivariable system, *directionality* will have to be considered [26]. From (28) the two interesting disturbances corresponding to the least controllable directions are potential energy, $\boldsymbol{E}_\mathrm{p} \triangleq E_\mathrm{p} + E_p'$, $\boldsymbol{z}_0 \in \mathrm{span}(\boldsymbol{v}_1)$; and kinetic energy, $\boldsymbol{E}_\mathrm{k} \triangleq E_\mathrm{k} + E_k'$, $\boldsymbol{z}_0 \in \mathrm{span}(\boldsymbol{v}_2)$. Interpreted as oscillatory energy, this becomes $\boldsymbol{E}_0 \triangleq \boldsymbol{E}_\mathrm{p} + \boldsymbol{E}_\mathrm{k}$, $\boldsymbol{z}_0 \in \mathrm{span}(\boldsymbol{v}_1, \boldsymbol{v}_2)$.

For small ϵ, networks will have similar modal frequencies, and controllability is going to be greatly affected by system interactions $\boldsymbol{\alpha}$, $\boldsymbol{\beta}$ and $\boldsymbol{\gamma}$. The smallest singular values of $\boldsymbol{W}_C$ corresponding to directions $\boldsymbol{v}_i$ with highest required control effort are the most interesting ones. Approximating these gives an analytical estimate of the controllability.

Making a Maclaurin series expansion of matrix elements (27) with respect to ϵ shows that for small ϵ

$$\left|\frac{d\boldsymbol{\alpha}(\epsilon)}{d\epsilon}\right| < \left|\frac{db'(\epsilon)}{d\epsilon}\right| < \left|\frac{d\boldsymbol{\beta}(\epsilon)}{d\epsilon}\right| < \left|\frac{d\boldsymbol{\gamma}(\epsilon)}{d\epsilon}\right|. \tag{29}$$

A simplification of $\boldsymbol{W}_C$, accurate for small ϵ, is then

$$\boldsymbol{W}_C^\gamma \triangleq \boldsymbol{W}_C(\boldsymbol{\alpha} = a,\, b' = b,\, \boldsymbol{\beta} = b). \tag{30}$$

where the smallest singular value becomes

$$\boldsymbol{\sigma}_\gamma \triangleq \min\left(\mathrm{svd}(\boldsymbol{W}_C^\gamma)\right) = \left|b - \sqrt{(b^2 + \boldsymbol{\gamma}^2)}\right|. \tag{31}$$

Maclaurin series expansion of $\boldsymbol{\sigma}_\gamma$ gives the estimate

$$\boldsymbol{\sigma}_\gamma(\epsilon) = \frac{X_B^2}{D}\frac{1}{2D^2M}\epsilon^2 + \mathcal{O}(\epsilon^3). \tag{32}$$

In Fig. 3 we let the networks Σ and Σ' be defined with $D = 2/\omega_s$, $f_s = 50$ Hz, $X_B = 0.5$, unit voltage, and unit line impedance such that their modal frequencies are $\omega_0 = \sqrt{2/M}$ and $\omega_0' = \sqrt{2/(M+\epsilon)}$, respectively. As seen in Fig. 3, (31) is only accurate for small ϵ. For slightly larger ϵ the properties of $\boldsymbol{W}_C$ is dominated by the diagonal blocks

$$\boldsymbol{W}_C^p \triangleq \begin{bmatrix} a & -\boldsymbol{\alpha} \\ -\boldsymbol{\alpha} & a \end{bmatrix} \text{ and } \boldsymbol{W}_C^k \triangleq \begin{bmatrix} b & -\boldsymbol{\beta} \\ -\boldsymbol{\beta} & b' \end{bmatrix} \tag{33}$$

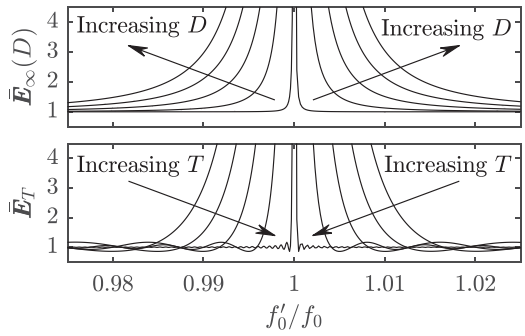

Fig. 4. The normalized minimal energy control (42) calculated using $\bar{\boldsymbol{E}}_\infty(D)$ (top) with $D = \{0.1, 1, 2, 3, 4\}/\omega_s$ and $\bar{\boldsymbol{E}}_T$ (bottom) with $D = 0$ and $T = \omega_s/\{0.1, 1, 2, 3, 4\}$. It follows that a more aggressive control comes at the cost of increased sensitivity to modal interaction.

in (25), where, the smallest singular value

$$\boldsymbol{\sigma}_p \triangleq \min\left(\mathrm{svd}(\boldsymbol{W}_C^p)\right) = |a - \boldsymbol{\alpha}| \tag{34}$$

together with (27) becomes

$$\boldsymbol{\sigma}_p(\epsilon) = \frac{X_B^2}{D}\frac{X_{12}}{2V^2}\frac{2c\epsilon^2}{2M + \epsilon + 2c\epsilon^2}. \tag{35}$$

For the second-order term of (35) to match that of (32), c in (35) needs to be replaced by $c/2$, suggesting the estimate

$$\boldsymbol{\sigma}_1(\epsilon) \approx \frac{X_B^2}{D}\frac{X_{12}}{2V^2}\frac{c\epsilon^2}{2M + \epsilon + c\epsilon^2}. \tag{36}$$

C. Modal Interaction and Energy Interpretation

From (11) and (26) it follows that

$$\epsilon = \frac{2V^2}{X_{12}\omega_0'^2} - M. \tag{37}$$

Substituting (37) in (36), the control effort required for an initial disturbed state, $\boldsymbol{z}_0 \in \mathrm{span}(\boldsymbol{v}_1)$ becomes

$$\|\boldsymbol{u}\|_2^2 \approx \boldsymbol{E}_p \frac{D}{X_B^2}\left(1 + D^2\frac{1 + f_0^2/f_0'^2}{\frac{2V^2M}{X_{12}}(1 - f_0^2/f_0'^2)^2}\right) \tag{38}$$

where $\boldsymbol{E}_p = \boldsymbol{v}_1^\mathsf{T}\frac{2V^2}{X_{12}}\boldsymbol{v}_1$. But as implied by (24) and (28), (38) holds for any $\boldsymbol{z}_0 \in \mathrm{span}(\boldsymbol{v}_1, \boldsymbol{v}_2)$ and any network Σ and Σ'. Defining

$$\boldsymbol{\Psi} \triangleq 1 + D^2\frac{1 + f_0^2/f_0'^2}{\boldsymbol{\rho}(1 - f_0^2/f_0'^2)^2},\ \boldsymbol{\rho} \triangleq 2\sqrt{\frac{V^2M}{X_{12}}\frac{V'^2M'}{X_{12}'}}$$

$$\boldsymbol{\Psi}' \triangleq 1 + D^2\frac{1 + f_0'^2/f_0^2}{\boldsymbol{\rho}(1 - f_0'^2/f_0^2)^2} \tag{39}$$

allows us to express the worst-case required control effort due to modal interaction between the HVDC-interconnected ac networks as

$$\|\boldsymbol{u}\|_2^2 \approx \boldsymbol{E}_\infty^2(D) \triangleq \boldsymbol{E}_0\frac{D}{X_B^2}\sqrt{\boldsymbol{\Psi}\boldsymbol{\Psi}'}. \tag{40}$$

In Fig. 4 the estimate (40) is compared with numerical results using a finite-time controllability Gramian (17) for an

undamped system

$$\boldsymbol{E}_T^2 \triangleq \boldsymbol{z}_0^\mathsf{T} \left(\int_0^T e^{\boldsymbol{A}_z t} \boldsymbol{B}_z \boldsymbol{B}_z^\mathsf{T} e^{\boldsymbol{A}_z^\mathsf{T} t} dt \right)^{-1} \boldsymbol{z}_0 \tag{41}$$

where $\boldsymbol{z}_0 \in \text{span}(\boldsymbol{v}_1, \boldsymbol{v}_2)$ and we let T be the inverse of the damping constant D used in (40). The measures, (40) and (41) are normalized as

$$\bar{\boldsymbol{E}}_\infty(D) \triangleq \sqrt{\boldsymbol{\Psi}\boldsymbol{\Psi}'} \text{ and } \bar{\boldsymbol{E}}_T \triangleq \frac{\boldsymbol{E}_T^2}{E_T^2 + E_T'^2} \tag{42}$$

where E_T^2 and $E_T'^2$ are the corresponding finite-time minimal control effort (41) for Σ and Σ', respectively.

In Fig. 4 it is shown how the modal interaction puts a limit to how aggressive the control action can be. An inverse relation between D and T is seen. This indicates that D is a reasonable representation of control aggressiveness.

V. Control Synthesis

Consider the HVDC-interconnected system depicted in Fig. 1. The input $\boldsymbol{u} = P_{\text{DC}}$ is controlled with proportional feedback. Neglecting the HVDC actuation lag, the following control law is used:

$$\boldsymbol{u} = P_{\text{DC}}^0 + \boldsymbol{K}\boldsymbol{y}. \tag{43}$$

Here we propose the feedback signal $\boldsymbol{y} = \begin{bmatrix} \omega_1 - \omega_2, \ \omega_1' - \omega_2' \end{bmatrix}$ to target the oscillatory energy in each system. For simplicity a proportional droop controller, $\boldsymbol{K} = \begin{bmatrix} K, \ -K' \end{bmatrix}$ is considered. For load disturbances, this controller should yield a good trade-off between output performance and input usage [26].

When controlling an isolated ac network, POD increases linearly with feedback gain. However, for the HVDC-interconnected system the overall performance, if measured by the least controllable direction, deteriorates as the feedback gain increases. Sensitivity to high feedback gain increases when $f_0/f_0' \to 1$ as seen in (38)–(40). This indicates that the HVDC-interconnected system has an optimal feedback gain $\boldsymbol{K}$ where a trade-off between increased damping and deterioration of controllability in both ac networks is met.

We now implement a simple pole placement algorithm where $\boldsymbol{K}$ is designed to maximize the minimal system damping ratio

$$\zeta_{\min} \triangleq \min_{i=1,2,3,4} \{\zeta_i = -\Re(\lambda_i)/|\lambda_i|\}. \tag{44}$$

where $\lambda_i, \ i = 1, 2, 3, 4$ are the eigenvalues of the closed-loop system

$$\dot{\boldsymbol{z}} = \boldsymbol{A}_z \boldsymbol{z} - \boldsymbol{B}_z \boldsymbol{K} \boldsymbol{H}_z \boldsymbol{z}. \tag{45}$$

This control strategy requires that a good estimate of $\boldsymbol{y}$ is available, which could be obtained using local or external measurements. For the simulation study, we assume that $\boldsymbol{H}_z$ gives the desired feedback signal scaled with the observability from local frequency measurements at the dc terminals. The optimal feedback gain is then obtained by solving

$$\max_{\boldsymbol{K}} \ \zeta_{\min} \quad \text{s.t. } K, K' \geq 0. \tag{46}$$

TABLE I
The Considered Cases Ξ_j Together With Optimal Gain and Damping Obtained for Simplified and Detailed Model. These Results Only Consider Accurate Parameter Estimates

Case	Ξ_1		Ξ_2		Ξ_3		Ξ_4	
Network	Σ	Σ'	Σ	Σ'	Σ	Σ'	Σ	Σ'
f_0 [Hz]	0.5	0.525	0.5	0.6	0.5	0.6	0.5	0.6
H [s]	6	6	6	6	4	6	6	6
X_B	0.5	0.5	0.5	0.5	0.5	0.5	0.8	0.5
$\hat{\boldsymbol{K}}$ [s]	0.18	0.20	0.69	0.83	0.44	0.82	0.27	0.83
$\hat{\zeta}_{\min}$ [%]	2.9		9.4		9.2		9.4	
$\zeta_{\min}$ [%]	2.2		7.0		6.9		7.0	
$\boldsymbol{K}^*$ [s]	0.17	0.18	0.66	0.79	0.42	0.76	0.26	0.79
$\zeta_{\min}^*$ [%]	2.7		9.2		9.0		9.2	

A. Detailed Model Specification

To illustrate the control strategy on a more detailed system, we consider a HVDC-interconnected system where each network is represented by a two-machine model where

- the nonlinear dynamics given by (1), (2) are considered;
- we allow asymmetric networks with $X_B \neq X_B'$ and

$$M_1 \triangleq M, \ M_2 \triangleq \alpha M; \tag{47}$$

- each machine is equipped with primary frequency control, whose active-power injection is given by the first-order governor

$$P_{m,i} = P_{m,i}^0 - \frac{1}{sT_g + 1} \frac{R_g}{\omega_s} \omega_i \tag{48}$$

  with time constant $T_g = 2$ s and droop gain $R_g = 25$ p.u. for all machines and;
- HVDC is utilized to share primary frequency reserves by adding the additional primary control to (43)

$$\Delta P_{\text{DC}} = \frac{1}{sT_{\text{DC}} + 1} \frac{R_{\text{DC}}}{\omega_s} (\omega_{\text{COI}} - \omega_{\text{COI}}') \tag{49}$$

  where $T_{\text{DC}} = 2$ s and $R_{\text{DC}} = 50$ p.u.

The controllability analysis done in Section IV and the control strategy (46) are based on a simplified model where higher-order dynamics such as primary frequency control, (48) and (49), are lumped into the damping constant D. The effect of the unmodeled dynamics is studied by synthesizing a controller based on the simplified system (16). Performance, in terms of POD, will then be compared between the simplified and the detailed model.

Four cases, $\Xi_j, \ j = 1, 2, 3, 4$ of HVDC-interconnected ac networks Σ and Σ' as specified in Table I are considered. The system parameters are given in per unit (p.u.). Common to all cases is that we let $D = D' = 2/\omega_s$, $\alpha = 1$, and primary control at machines and dc terminals as specified by (48) and (49). Machine inertia constant $M = 2HS_r/\omega_s$ are based on the inertia time constant H, which usually falls within 3–8 s for a power system dominated by synchronous machines [2]. Rated power of each machine is set to $S_r = 4$ p.u., $f_s = f_s' = 50$ Hz, and $V = V' = 1$ p.u. Network impedance is given by (11) such that $\omega_0 = 2\pi f_0$ for the specific case Ξ_j. As an example, $\begin{bmatrix} X_{12}, \ X_{12}' \end{bmatrix} \approx \begin{bmatrix} 1.3, \ 1.2 \end{bmatrix}$ for Ξ_1. The active

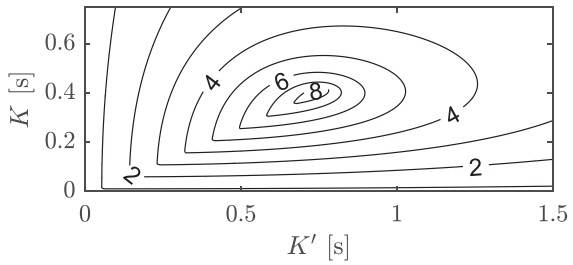

Fig. 5. Case Ξ_3: Level curves for the minimal system damping ratio $\zeta_{\min}$ [%] as a function of both K and K'.

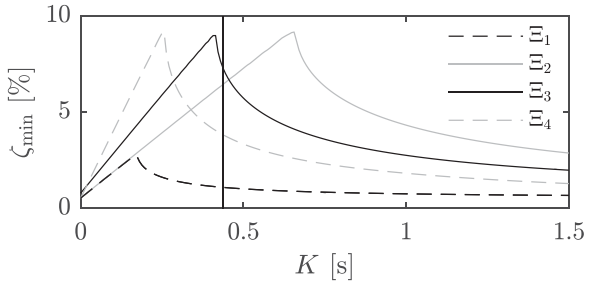

Fig. 6. Cases Ξ_j: The highest minimal system damping ratio $\zeta_{\min}$ as a function of K. Vertical line indicates optimal $\hat{K}$ obtained from the simplified model in Ξ_3.

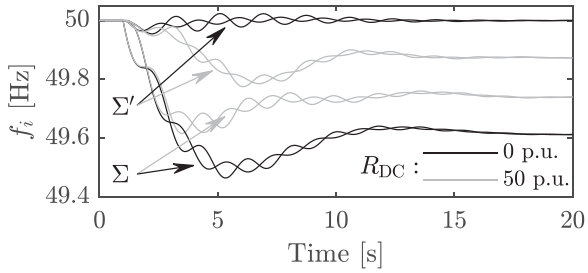

Fig. 7. Case Ξ_1: Machine speeds following a 0.4-% load increase in Network Σ (bottom line-pair) aided by Network Σ' (top line-pair). Gray and black lines shows performance with and without sharing of primary reserves through the HVDC link (49), respectively.

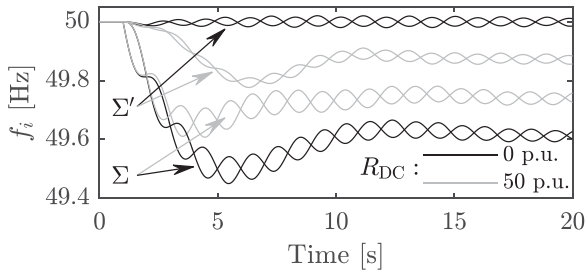

Fig. 8. Case Ξ_2: Scenario identical to Fig. 7.

power injection is consumed locally at each machine bus. Hence, $\Delta P_i = P_{ei} = P^0_{\mathrm{DC}} = 0,\ \forall i$.

B. Tuning Controller From Reconstructed Model

To investigate the sensitivity to unmodeled dynamics we assume that the only information available is the estimated eigenvalues $\hat{\lambda}_i = -\hat{\gamma}_i \pm j\hat{\omega}_{ei}$. In particular interest are the eigenvalues $\hat{\lambda}_1$ and $\hat{\lambda}'_1$ representing the poorly damped interarea mode in network Σ and Σ', respectively. Using this information, a model of the reduced networks Σ and Σ' (10) is reconstructed by solving the characteristic equation of A_z:

$$\ddot{\delta} + \underbrace{\frac{D}{M_{12}}}_{2\gamma}\dot{\delta} + \underbrace{\frac{V^2 M_{12}}{M_1 M_2 X_{12}}}_{\omega_0^2}\delta = 0. \tag{50}$$

Since the mode is poorly damped, we assume $\omega_e \approx \omega_0$. Proposing some parameter estimates $\hat{H}$, $\hat{X}_B$, and $\hat{\alpha}$ allows us to recreate (10). Optimal POD gains $\hat{\boldsymbol{K}}$ are obtained using (46) for the simplified model. In Table I it is seen that the controller gains $\hat{\boldsymbol{K}}$ result in slightly lower POD when applied to the detailed model ($\zeta_{\min} < \hat{\zeta}_{\min}$). Comparing $\hat{\boldsymbol{K}}$ with the optimal gain obtained for the detailed system $\boldsymbol{K}^*$, we see that a good conservative approach to account for these unmodeled dynamics would be to scale $\hat{\boldsymbol{K}}$ with some factor smaller than one. The main reason for POD deterioration is the HVDC primary control (49), which could be taken into account in the tuning process.

Fig. 5 shows the minimal system damping ratio $\zeta_{\min}$ for Ξ_3 as a function of both K and K' while Fig. 6 shows the highest $\zeta_{\min}$ achieved at each given K. In Fig. 6 it is seen that lowering the inertia, or moving the dc bus location closer to one of the generator as in Ξ_3 and Ξ_4, respectively, makes Σ more controllable. Feedback gain K consequently have a higher effect on POD in Σ. However, its seen that only the frequency ratio f_0/f'_0 will have a significant effect on optimal performance as indicated in Section IV-C. Consequently, this means a lower K for the more controllable cases.

As seen in Table I and Fig. 6, the model reconstruction proposed in Section V-B does not give optimal performance with the tuning method (46) due to unmodeled dynamics.

VI. Simulations Study of POD

MATLAB simulations using the model considered in Section V-A are presented next. A disturbance in the form of a sudden 0.4 p.u. load increase at machine-bus 1 in Σ is the considered scenario.

Machine speeds with feedback gain $\hat{\boldsymbol{K}}$ obtained from the simplified model, using the procedure introduced in Section V-B, are presented in Figs. 7 and 8 for Ξ_1 and Ξ_2, respectively.

An immediate frequency fall can be seen at machine-bus 1 in Σ where the load increase occurs. The load imbalance causes a separation in machine speeds and an ensuing power oscillation between the two machines of Σ. The proposed control scheme (45) is implemented to increase POD, consequently spreading the power oscillation to the assisting network. A larger difference between f_0 and f'_0 gives a lower modal interaction between the networks according to Section IV-C. Hence, Ξ_2 facilitates a higher POD performance compared to Ξ_1. A higher feedback gain moves f_0 and f'_0 closer to each other. As the modal fre-

TABLE II
SENSITIVITY TO PARAMETER ESTIMATE $\hat{X}_B$ WITH $R_{\mathrm{DC}} = 0$

Case	$\hat{X}_B$	$\hat{K}$	$\hat{K}'$ [s]	$\hat{\zeta}_{\min}$	ζ_0	ζ_0' [%]
Ξ_2	0.5	0.69	0.83	9.4	9.9	8.8
$\Xi_{2,a}$	0.25	2.75	0.83	9.4	44	1.5
$\Xi_{2,b}$	0.75	0.31	0.83	9.4	3.8	10
$\Xi_{2,0}$	-	-	-	-	0.52	0.39

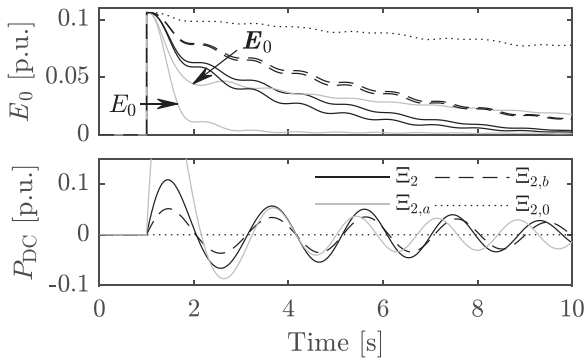

Fig. 9. Oscillatory energy (top) following a 0.4 p.u. load increase in Σ for the cases specified in Table II, with the resulting P_{DC} (bottom). Per unit energy is calculated using (14), where the potential energy is in relation to pre- and post-disturbed steady state.

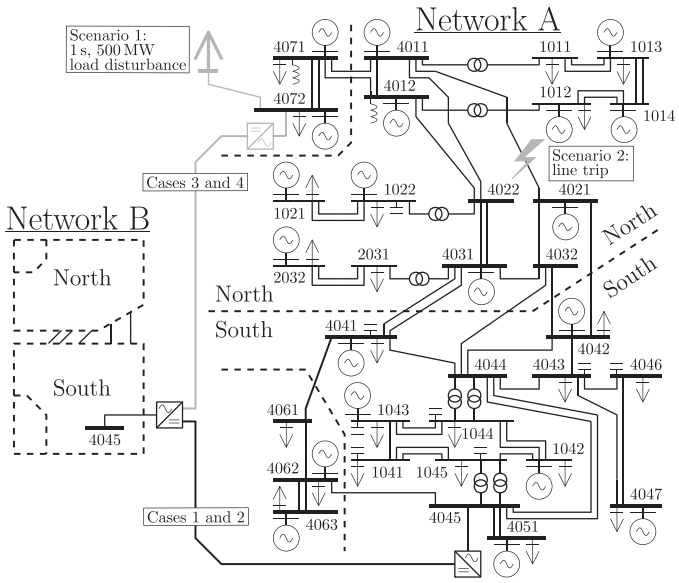

Fig. 10. Simulation model implemented in Simulink consisting of two HVDC-interconnected Nordic-32 networks [27].

quencies move closer to each other, controllability and thus, POD benefits are reduced.

To illustrate the effect of primary control (49) we also consider a model with $R_{\mathrm{DC}} = 0$ in both cases. Comparing the cases with primary control (gray lines), to those without (black lines) we see that sharing of primary reserves, to reduce nadir and steady state frequency deviation, can be implemented independent of POD control.

A. Sensitivity to Parameter Estimates

In Section V-B it was seen that system parameters affect controllability. To show the effect of misjudging the dc busbar location in the tuning process, we consider Ξ_2 with two different estimates of $\hat{X}_B$, given in Table II. The effect on POD is clarified by setting $R_{\mathrm{DC}} = 0$.

In $\Xi_{2,a}$, an overestimated $\hat{K}$ greatly increases POD performance in Σ at the cost of overall system performance, measured by $\boldsymbol{\zeta}_{\min}$. This is shown in Fig. 9 using the same disturbance scenario as in Section VI. Instead of showing the machines speeds however, Fig. 9 shows the oscillatory energy (14) following the disturbance. The oscillatory energy E_0 in the disturbed network is greatly reduced due to a high initial P_{DC}. This however, introduce a large oscillatory energy E_0' in the assisting network where the POD is lower, reducing overall system performance.

Underestimating $\hat{K}$ in $\Xi_{2,b}$ gives the opposite result, as shown in Table II and Fig. 9. Case $\Xi_{2,0}$ gives an additional comparison where POD control is not utilized. From $\Xi_{2,0}$ we see that even though badly tuned $\boldsymbol{K}$ gives poor POD, we can always expect an improvement from the case without POD control.

B. Simulation Study on Two Nordic 32-Bus Models

To improve the confidence in the analytical results, simulations on more detailed power system models are made in Simulink. The considered system is two HVDC-interconnected Nordic 32-bus Cigré test systems (N32) [27] seen in Fig. 10. The N32 model is a system with large power transfers from the hydro dominated north and external areas (lumped into north area) to loads in the central and southwestern areas (lumped into the south area) where a large amount of thermal power is installed. For the study, the two networks (A and B) are interconnected using two different HVDC configurations, as seen in Fig. 10.

The implemented N32 model shows a 0.50 Hz interarea mode between the north and south areas. For illustrative purposes, the damping of this mode is reduced to roughly 1% by modifying the PSS at machines 4072 and 1042. The HVDC active power is modulated using (45) with the relative frequency difference $y = \frac{\sum_{i\in\text{south}} M_i\omega_i}{\sum_{i\in\text{south}} M_i} - \frac{\sum_{i\in\text{north}} M_i\omega_i}{\sum_{i\in\text{north}} M_i}$ as feedback signal from each network. The signal is obtained by communicating the machine measurements to the dc controller. A proportional controller is implemented using the tuning procedure introduced in Section V. The second-order system representation (8), used in the tuning process, is obtained using Simulink's Linear Analysis Tool.

Four cases with different system topologies are considered. In case 1 and 2 the dc link is located at bus 4045 in both ac networks. In case 3 and 4 the dc terminal is moved to bus 4072 in network A. To illustrate limitations imposed by modal interaction, the inertia time constants are scaled to modify modal frequencies (11) of network B. The cases are summarized in Table III.

The result shown in Table IV confirms the analytic result that modal interaction limits the potential POD benefits from active power modulation. The control, tuned to each specific case, exploits the modal frequencies. With higher gains they move closer to each other and the system lose controllability of the interarea modes. Moving the dc terminal to the more controllable position at bus 4072 in case 3 and 4 reduces the required dc

TABLE III
MODAL FREQUENCIES AND DC BUSES OF THE FOUR CONSIDERED CASES OF HVDC-INTERCONNECTED N32 NETWORKS

Case	1		2		3		4	
Network	A	B	A	B	A	B	A	B
f_0 [Hz]	0.51	0.53	0.51	0.60	0.51	0.53	0.51	0.60
DC Bus	4045	4045	4045	4045	4072	4045	4072	4045

TABLE IV
RESULTING POD OF THE HVDC-INTERCONNECTED N32 NETWORKS. CONTROLLER K_i IS TUNED TO THE CORRESPONDING CASE i

Controller	K_1	K_2	K_3	K_4
Gain [MW/Hz]	453 617	1558 1675	190 514	663 1410
$\hat{\zeta}_{\min}$ [%]	3.4	9.4	3.2	8.6
$\zeta_{\min}$(Case 1) [%]	2.9	1.4	1.8	1.6
$\zeta_{\min}$(Case 2) [%]	3.0	6.9	1.8	3.7
$\zeta_{\min}$(Case 3) [%]	1.5	0.9	2.9	1.1
$\zeta_{\min}$(Case 4) [%]	4.2	3.0	3.0	7.1

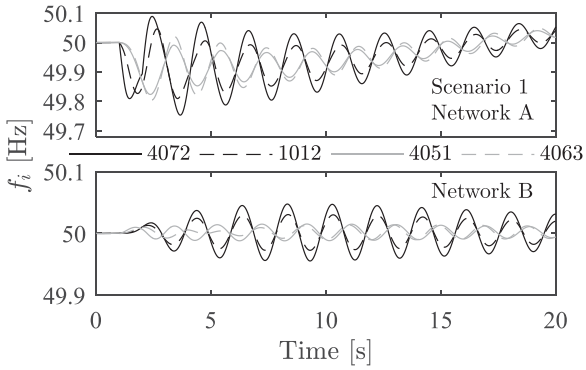

Fig. 11. Scenario 1: Machine speeds at buses 4072 and 1012 in the northern areas and 4051 and 4063 in the southern areas following a 500 MW load disturbance at bus 4072 in network A.

power actuation but have negligible effect on resulting POD performance. To verify the results, simulations of the nonlinear system where made.

Scenario 1) Load Disturbance, Case 1, Controller K_1: A 500 MW load disturbance occur at the time interval $t = [1, 2]$ s at bus 4072 in network A. As shown in Fig. 11 the load disturbance reduces the initial machine speed at bus 4072 ensuing in a north–south interarea oscillation.

Scenario 2) Line Trip, Case 2, Controller K_2: The transmission line between buses 4011 and 4021 is tripped at time $t = 1$ s. Since there is a large power transfer from the north to the south, the initial loss of transfer capacity causes machines in the north area to accelerate while the southern machines decelerate. As seen in Fig. 12 a local mode within the north area is also excited by the disturbance. However, the local mode is well damped and after a while the response is dominated by the north–south interarea mode.

Resulting HVDC active power for the two scenarios is shown in Fig. 13. HVDC active power modulation is shown to be effective in both scenarios. In agreement with previous analysis it is also seen that case 2, with higher modal ratio, allows for a higher feedback gain and a higher POD improvement than case 1.

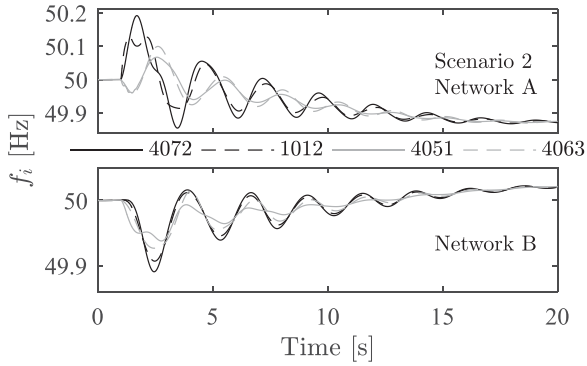

Fig. 12. Scenario 2: Machine speeds at buses 4072 and 1012 in the northern areas and 4051 and 4063 in the southern areas following a line trip in the northern area of network A.

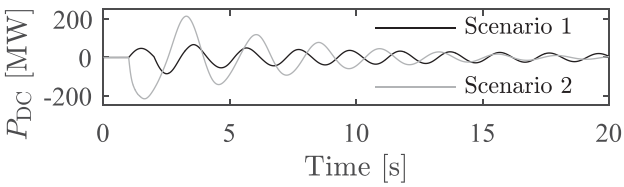

Fig. 13. HVDC active power following the disturbance of the two scenarios in Figs. 11 and 12.

VII. CONCLUSIONS

It was shown that, for a controllable HVDC-interconnected system, local frequency feedback may improve POD regardless of gain, verifying the findings of [5]. If the dynamics of the power source can be neglected then performance is essentially only limited by the available power. The focus of this work have been to increase the understanding on the fundamental factors limiting achievable performance when dynamical interactions can not be neglected.

In Sections IV-C and VI-B it was shown that the ratio between modal frequencies gives a fundamental limit to achievable performance. By lowering the feedback gain, differences in open-loop modal frequencies between the interconnected systems can be used to increase system performance in terms of POD. If the implemented control is to aggressive, the interarea oscillations of the two systems will essentially be synchronized. High feedback would allow the networks to share inertial response following disturbances which might be beneficial with regards to transient stability. However, if POD is desired, then feedback gains are limited by the modal interaction. This is because the disturbance propagate and excite the interarea mode in the neighboring system. This could be mitigated if energy storage, e.g., from dc capacitors are available. Cooperative control of multiple HVDC links or a multi-terminal HVDC (MTDC) can be another way of circumventing the observed limitations.

In this study we considered POD of one dominant interarea mode in each ac network. Future work will extending these results to a network with multiple ac modes. Possible interaction with dc dynamics will also be considered. In addition, cooperative control of multiple links and MTDC networks will be addressed. In particular, communication and robustness to inverter pole outages will be of interest since this may limit the potential benefits. If communication and reliable operation can

not be guaranteed, then the modal interaction is likely going to be a limiting factor for such a system as well.

ACKNOWLEDGMENT

The authors would like to thank Prof. Henrik Sandberg, KTH Royal Institute of Technology, Dr. Bertil Berggren, Principal Scientist at ABB, and Dr. Robert Eriksson, R&D coordinator at Svenska kraftnät (Swedish National Grid), for valuable discussions and comments to this work.

REFERENCES

[1] P. Kundur *et al.*, "Definition and classification of power system stability IEEE/CIGRE joint task force on stability terms and definitions," *IEEE Trans. Power Syst.*, vol. 19, no. 3, pp. 1387–1401, Aug. 2014.
[2] P. Kundur, *Power System Stability and Control*. New York, NY, USA: McGraw-Hill, 1994.
[3] A. T. Gullberg, D. Ohlhorst, and M. Schreurs, "Towards a low carbon energy future—Renewable energy cooperation between Germany and Norway," *Renew. Energy*, vol. 68, pp. 216–222, Aug. 2014.
[4] L. Harnefors, N. Johansson, L. Zhang, and B. Berggren, "Interarea oscillation damping using active-power modulation of multiterminal HVDC transmissions," *IEEE Trans. Power Syst.*, vol. 29, no. 5, pp. 2529–2538, Sep. 2014.
[5] L. Harnefors, N. Johansson, and L. Zhang, "Impact on interarea modes of fast HVDC primary frequency control," *IEEE Trans. Power Syst.*, vol. 32, no. 2, pp. 1350–1358, Mar. 2017.
[6] T. Smed and G. Andersson, "Utilizing HVDC to damp power oscillations," *IEEE Trans. Power Del*, vol. 8, no. 2, pp. 620–627, Apr. 1993.
[7] R. Eriksson, "A new control structure for multiterminal dc grids to damp interarea oscillations," *IEEE Trans. Power Del.*, vol. 31, no. 3, pp. 990–998, Jun. 2016.
[8] R. Eriksson, "Coordinated control of HVDC links in transmission systems," Ph.D. dissertation, KTH Royal Inst. Technol., Stockholm, Sweden, 2011.
[9] K. Tomiyama, M. Sato, K. Yamaji, M. Sekita, and M. Goto, "Power swing damping control by HVDC power modulation in an ac/dc hybrid transmission system," *Elect. Eng. Japan*, vol. 124, no. 3, pp. 10–18, 1998.
[10] J. J. Sanchez-Gasca and J. H. Chow, "Power system reduction to simplify the design of damping controllers for interarea oscillations," *IEEE Trans. Power Syst.*, vol. 11, no. 3, pp. 1342–1349, Aug. 1996.
[11] Y. Li, C. Rehtanz, D. C. Yang, K. Görner, S. Rüberg, and L. F. Luo, "Wide-area time-delay damping control to prevent power oscillations in HVDC/AC interconnected power systems," in *Proc. Int. Conf. Power Syst. Technol.*, Hangzhou, China, 2010, pp. 1–6.
[12] R. L. Cresap, W. A. Mittelstadt, D. N. Scott, and C. W. Taylor, "Operating experience with modulation of the Pacific HVDC Intertie," *IEEE Trans. Power App. Syst.*, vol. PAS-97, no. 4, pp. 1053–1059, Jul. 1978.
[13] C. W. Taylor and S. Lefebvre, "HVDC controls for system dynamic performance," *IEEE Trans. Power Syst.*, vol. 6, no. 2, pp. 743–752, May 1991.
[14] D. Trudnowski, D. Kosterev, and J. Undrill, "PDCI damping control analysis for the western North American power system," in *Proc. IEEE Power Energy Soc. Gen. Meeting*, Vancouver, BC, Canada, 2013, pp. 1–5.
[15] A. Banerjee and N. R. Chaudhuri, "Robust damping of inter-area oscillations in AC-MTDC grids using H∞ mixed-sensitivity approach," in *Proc. IEEE Power Energy Soc. Gen. Meeting*, Boston, MA, USA, 2016, pp. 1–5.
[16] M. A. Elizondo *et al.*, "Interarea oscillation damping control using high voltage dc transmission: A survey," *IEEE Trans. Power Syst.*, vol. 33, no. 6, pp. 6915–6923, Nov. 2018.
[17] M. Ndreko, A. vad der Meer, M. Gibescu, B. G. Rawn, and M. A. M. M. vad der Meijden, "Damping power system oscillations by VSC-based HVDC networks: A North Sea grid case study," in *Proc. 12th Wind Integr. Workshop*, London, U.K., 2013, pp. 1–6.
[18] W. Wang, Y. Li, Y. Cao, U. Häger, and C. Rehtanz, "Adaptive droop control of VSC-MTDC system for frequency support and power sharing," *IEEE Trans. Power Syst.*, vol. 33, no. 2, pp. 1264–1274, Mar. 2018.
[19] Y. Cao *et al.*, "A virtual synchronous generator control strategy for VSC-MTDC system," *IEEE Trans. Energy Convers.*, vol. 33, no. 2, pp. 750–761, Jun. 2018.
[20] J. Anderson, "The control of a synchronous machine using optimal control theory," *Proc. IEEE*, vol. 59, no. 1, pp. 25–35, Jan. 1971.
[21] W. Du, Q. Fu, and H. Wang, "Strong dynamic interactions between multiterminal dc network and ac power systems caused by open-loop modal coupling," *IET Gener., Transmiss. Distrib.*, vol. 11, no. 9, pp. 2362–2374, Jun. 2017.
[22] W. J. Rugh, *Linear System Theory*, 2nd ed. Upper Saddle River, NJ, USA: Pearson, 1995.
[23] C.-T. Chen, *Linear System Theory and Design* (Oxford Series in Electrical and Computer engineering), 3rd ed. New York, NY, USA: Oxford Univ. Press, 1999.
[24] C. Nordling, *Physics Handbook for Science and Engineering*, 8th ed. Lund, Sweden: Studentlitteratur, 2006.
[25] D. Xue and Y. Chen, *Solving Applied Mathematical Problems with MATLAB*, 1st ed. Boca Raton, FL, USA: Chapman & Hall/CRC Press, 2008.
[26] S. Skogestad and I. Postlethwaite, *Multivariable Feedback Control: Analysis and Design*, 2nd ed. Chichester, U.K.: Wiley, 2005.
[27] M. Stubbe, "Long term dynamics phase II final report," Cigre, Tech. Rep. Task Force 38.08.08, Mar. 1995.

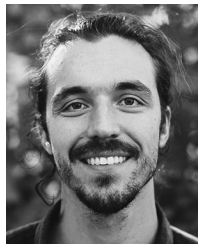

Joakim Björk (S'17) received the M.Sc. degree in energy systems engineering from Uppsala University, Uppsala, Sweden, in collaboration with the Swedish University of Agricultural Sciences, Uppsala, in 2016. He is working toward the Ph.D. degree with the Department of Automatic Control, KTH Royal Institute of Technology, Stockholm, Sweden.

His research interests include frequency and voltage control of power grids with focus on HVdc transmission.

Karl Henrik Johansson (F'13) received the M.Sc. and Ph.D. degrees from Lund University, Lund, Sweden.

He is the Director of the Stockholm Strategic Research Area ICT The Next Generation and a Professor with the School of Electrical Engineering and Computer Science, KTH Royal Institute of Technology. He has held visiting positions with the University of California, Berkeley, California Institute of Technology, Nanyang Technological University, HKUST Institute of Advanced Studies, and Norwegian University of Science and Technology. His research interests include networked control systems, cyber-physical systems, and applications in transportation, energy, and automation. He is a member of the IEEE Control Systems Society Board of Governors, the IFAC Executive Board, and the European Control Association Council. He has received several best paper awards and other distinctions. He has been awarded Distinguished Professor with the Swedish Research Council and Wallenberg Scholar. He is a recipient of the Future Research Leader Award from the Swedish Foundation for Strategic Research and the triennial Young Author Prize from IFAC. He is a Fellow of the Royal Swedish Academy of Engineering Sciences. He is an IEEE Distinguished Lecturer.

Lennart Harnefors (F'17) received the M.Sc., Licentiate, and Ph.D. degrees in electrical engineering from the KTH Royal Institute of Technology, Stockholm, Sweden, 1993, 1995, and 1997, respectively, and the Docent degree in industrial automation from Lund University, Lund, Sweden, in 2000.

Between 1994 and 2005, he was with Mälardalen University, Västerås, Sweden, where he became a Professor in 2001. Between 2001 and 2005, he was, in addition, a part-time Visiting Professor of electrical drives with the Chalmers University of Technology, Göteborg, Sweden. Since 2005, he has been with ABB, where he served in various capacities at the HVDC product group, Ludvika, Sweden, until 2012. He is currently a Senior Principal Scientist with ABB Corporate Research, Västerås. He is, in addition, a part-time Adjunct Professor of power electronics with the KTH Royal Institute of Technology. His research interests include analysis and control of power electronic systems, particularly grid-connected converters and ac drives. He is an Associate Editor for the IEEE TRANSACTIONS ON INDUSTRIAL ELECTRONICS and *IET Electric Power Applications.*